PERGAMON

Acta mater. 48 (2000) 223–238

Acta MATERIALIA

www.elsevier.com/locate/actamat

NANO-SCALE MATERIALS DEVELOPMENT FOR FUTURE MAGNETIC APPLICATIONS ☆

M. E. McHENRY and D. E. LAUGHLIN†

Department of Materials Science and Engineering, Data Storage Systems Center, Carnegie Mellon University, Pittsburgh, PA 15213, USA

(Received 1 June 1999; accepted 15 July 1999)

Abstract—Developments in the field of magnetic materials which show promise for future applications are reviewed. In particular recent work in nanocrystalline materials is reviewed, with either soft or hard behavior as well as advances in the magnetic materials used for magnetic recording. The role of microstructure on the extrinsic magnetic properties of the materials is stressed and it is emphasized how careful control of the microstructure has played an important role in their improvement. Important microstructural features such as grain size, grain shape and crystallographic texture all are major contributors to the properties of the materials. In addition, the critical role that new instrumentation has played in the better understanding of the nano-phase magnetic materials is demonstrated.

Keywords: Soft magnetic materials; Hard magnetic materials; Recording media; Microstructure; Nanophase

1. INTRODUCTION

Whether it can be called a revolution or simply a continuous evolution, it is clear that development of new materials and their understanding on a smaller and smaller length scale is at the root of progress in many areas of materials science [1]. This is particularly true in the development of new magnetic materials for a variety of important applications [2–5]. In recent years the focus has moved from the microcrystalline to the nanocrystalline regime. This paper intends to summarize recent developments in the synthesis, structural characterization, and properties of nanocrystalline and magnets for three distinct sets of magnetic applications:

1. Soft magnetic materials.
2. Hard magnetic materials.
3. Magnetic storage media.

The underlying physical phenomena that motivate these developments will be described. A unifying theme exists in the understanding of the relationships between microstructure and magnetic anisotropy (or lack thereof) in materials.

The term "nanocrystalline alloy" is used to describe those alloys that have a majority of grain diameters in the typical range from ~1 to 50 nm. This term will include alloys made by plasma processing [6–8], rapid solidification, and deposition techniques where the initial material may be in the amorphous state and subsequently crystallized. We discuss processing methods to control chemistry and microstructural morphology on increasingly smaller length scales, and various developing experimental techniques which allow more accurate and quantitative probes of structure on smaller length scales. We review the impact of microstructural control on the development of state of the art magnetic materials. Finally we offer a view to the future for each of these applications.

Over several decades, amorphous and nanocrystalline materials have been investigated for applications in magnetic devices requiring either magnetically hard or soft materials. In particular, amorphous and nanocrystalline materials have been investigated for various soft magnetic applications including transformers, inductive devices, etc. In these materials it has been determined that an important averaging of the magnetocrystalline anisotropy over many grains coupled within an *exchange length* is the root of the magnetic softness of these materials. The fact that this magnetic exchange

† To whom all correspondence should be addressed.

☆ The Millennium Special Issue — A Selection of Major Topics in Materials Science and Engineering: Current status and future directions, edited by S. Suresh.

PII: S1359-6454(99)00296-7

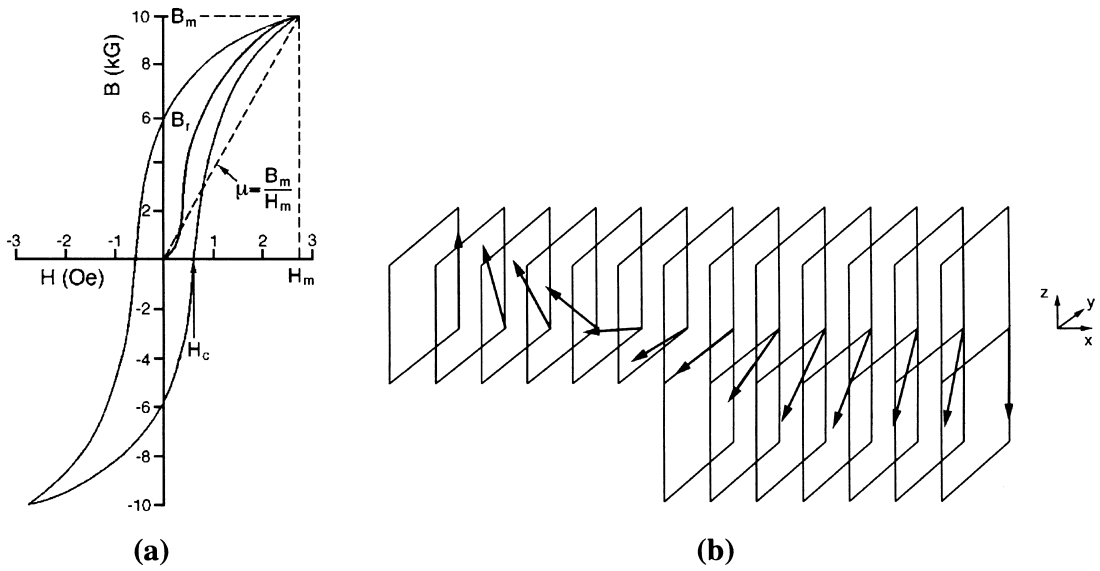

Fig. 1. (a) Schematic of a hysteresis curve for a magnetic material defining some technical magnetic parameters and (b) rotation of atomic magnetic dipole moments in a 180° (Bloch) domain wall in a ferromagnetic material.

length is typically nanometers or tens of nanometers illustrates the underlying importance of this length scale in magnetic systems.

In rare earth permanent magnets [9], it has been determined that a microstructure containing two or more phases, where the majority phase is nanocrystalline (taking advantage of the favorable high coercivity in particles of optimum size) and one or more of the phases are used to pin magnetic domain walls leads to better hard magnetic properties. Still another exciting recent development has been the suggestion of composite *spring exchange* magnets [10] that combine the large coercivities in hard magnets with large inductions found in softer transition metal magnets. Again chemical and structural variations on a nano-scale are important for determining optimal magnetic properties.

In the area of magnetic storage media future progress will also rely on the ability to develop control over microstructure at smaller size scales so as to impact on storage densities. Here the issue of thermal stability of the magnetic dipole moment of fine particles has become a critical issue, with the so-called superparamagnetic limit on the horizon. The need to store information in smaller and smaller magnetic volumes pushes the need to develop media with larger magnetocrystalline anisotropies.

2. DEFINITIONS

Technical magnetic properties [11, 12] can be defined making use of a typical magnetic hysteresis curve as illustrated in Fig. 1. Magnetic hysteresis [Fig. 1(a)] is a useful attribute of a permanent magnet material in which we wish to store a large metastable magnetization. Attributes of a good permenent magnet include: (a) large saturation and remnant inductions, B_s and B_r: a large saturation magnetization, M_s, and induction, B_s, are desirable in applications of both hard (and soft) magnetic materials; (b) large coercivities, H_c: coercivity is a measure of the width of a hysteresis loop and a measure of the permanence of the magnetic moment; (c) high Curie temperature, T_c: the ability to use soft magnetic materials at elevated temperatures is intimately dependent on the Curie temperature or magnetic ordering temperature of the material.

A large class of applications requires small hysteresis losses per cycle. These are called soft magnetic materials and their attributes include: (a) high permeability: permeability, $\mu = B/H = (1 + \chi)$, is the material's parameter which describes the flux density, **B**, produced by a given applied field, **H**. In high permeability materials we can produce very large changes in magnetic flux density in very small fields; (b) low hysteresis loss: hysteresis loss represents the energy consumed in cycling a material between fields H and $-H$ and back again. The energy consumed in one cycle is $W_H = \oint M \, dB$ or the area inside the hysteresis loop. The hysteretic power loss of an a.c. device includes a term equal to the frequency multiplied by the hysteretic loss per cycle; (c) large saturation and remnant magnetizations; (d) high Curie temperatures.

The magnetization curve [Fig. 1(a)] illustrates the technical magnetic properties of a ferromagnetic material. Its shape is determined by minimizing the material's magnetic free energy. The magnetic free energy consists of terms associated with the field

energy (Zeeman energy), self-field (demagnetization energy), wall energy, and magnetic anisotropy energy. The magnetic Helmholtz free energy [13] can be determined by integrating a magnetic energy density as follows:

$$F_{\mathrm{M}} = \int \left[A(\mathbf{r}) \left[\frac{\nabla \mathbf{M}}{\mathbf{M}_{\mathrm{s}}} \right]^2 - K_1(\mathbf{r}) \left[\frac{\mathbf{M} \cdot \mathbf{n}}{\mathbf{M}_{\mathrm{s}}} \right]^2 - \mu_0 \mathbf{M} \cdot \mathbf{H} \right] \mathrm{d}\mathbf{r} \tag{1}$$

where $A(\mathbf{r})$ is the local exchange stiffness related to the exchange energy, J and spin dipole moment, S ($A = CJS^2/a$ at 0 K, with $C \sim 1$ depending on crystal structure and a is the interatomic spacing), $K_1(\mathbf{r})$ is the (leading term) local magnetic anisotropy energy density, $\mathbf{M}$ is the magnetization vector, $\mathbf{n}$ is a unit vector parallel to the easy direction of magnetization, and $\mathbf{H}$ is the sum of the applied field and demagnetization field vectors. The magnetic anisotropy energy describes the angular dependence of the magnetic energy, i.e. its dependence on angles θ and ϕ between the magnetization and an easy axis of magnetization. For the case of a uniaxial material the leading term in the anisotropy energy density has a simple $K_1 \sin^2 \theta$ form. The anisotropy energy can be further subdivided into *magnetocrystalline, shape and stress anisotropies*, etc. For the purposes of the discussions here, however, we will devote most of our attention to the magnetocrystalline anisotropy.

The magnetic anisotropy represents a barrier to switching the magnetization. For soft magnetic materials, a small magnetic anisotropy is desired so as to minimize the hysteretic losses and maximize the permeability. In soft materials, the desire for small magnetocrystalline anisotropy necessitates the choice of cubic crystalline phases of Fe, Co, Ni or alloys such as FeCo, FeNi, etc. (with small values of K_1). In crystalline alloys, such as permalloy or FeCo, the alloy chemistry is varied so that the first-order magnetocrystalline anisotropy energy density, K_1, is minimized. Similarly, stress anisotropy is reduced in alloys with nearly zero magnetostriction. Shape anisotropy results from demagnetization effects and is minimized by producing materials with magnetic grains with large aspect ratios. Amorphous alloys are a special class of soft materials where (in some notable cases) low magnetic anisotropies result from the lack of crystalline periodicity.

For hard magnetic materials a large magnetic anisotropy is desirable. As discussed below, large magnetocrystalline anisotropy results from an anisotropic (preferably uniaxial) crystal structure, and large spin orbit interactions. Large magnetocrystalline anisotropy is seen, for example in h.c.p. cobalt, in CoPt where spin–orbit coupling to the relativistic Pt electrons invokes large anisotropies, and importantly in the rare earth permanent magnet materials.

In future discussions we will find it useful to describe several length scales that are associated with magnetic domains and domain walls [Fig. 1(b)]. These are expressed through consideration of domain wall energetics. The energy per unit area in the wall can be expressed as a sum of exchange and anisotropy energy terms:

$$\gamma_{\mathrm{W}} = \gamma_{\mathrm{ex}} + \gamma_K \tag{2}$$

where the anisotropy energy per unit volume, K, is multiplied by volume contained in a domain wall, $A_{\mathrm{W}}\delta_{\mathrm{W}}$, and divided by cross-sectional area to arrive at an anisotropy energy per unit area:

$$\gamma_K = K\left(\frac{A_{\mathrm{W}}\delta_{\mathrm{W}}}{A_{\mathrm{W}}}\right) = K\delta_{\mathrm{W}} = K(Na) \tag{3}$$

where $\delta_{\mathrm{W}} = Na$ (a is the lattice constant in the direction of rotation and N is the number of planes over which the rotation takes place) is the thickness of the wall. Thus γ_{W} can be expressed as

$$\gamma_{\mathrm{W}} = \frac{\pi^2 J_{\mathrm{ex}} S^2}{Na^2} + K_1(Na) \tag{4}$$

where the first term considers the cost in exchange energy in rotating magnetic dipole moments in a 180° domain wall as illustrated in Fig. 1(b). To determine the optimal wall thickness we differentiate γ_{W} with respect to δ_{W} yielding:

$$N_{\mathrm{eq}} = \sqrt{\frac{\pi^2 J_{\mathrm{ex}} S^2}{K_1 a^3}}. \tag{5}$$

For Fe, $N_{\mathrm{eq}} \sim 300$ and the equilibrium thickness, $t_{\mathrm{eq}} = N_{\mathrm{eq}}a \sim 50$ nm. Expressed in terms of the exchange stiffness, A_{ex}, and the domain wall width, $\delta_{\mathrm{W}} = \pi\sqrt{A_{\mathrm{ex}}/K_1}$.

Another important length scale is the distance over which the perturbation due to the switching of a single spin decays in a soft material. This length is called the ferromagnetic exchange length, L_{ex}, and can be expressed as

$$L_{\mathrm{ex}} = \sqrt{\frac{A_{\mathrm{ex}}}{\mu_0 M_{\mathrm{s}}^2}}. \tag{6}$$

The ferromagnetic exchange length is ~3 nm for ferromagnetic iron- or cobalt-based alloys. The ratio of the exchange length to δ_{W}/π is a dimensionless parameter, κ, called the magnetic hardness parameter:

$$\kappa = \frac{\pi L_{\mathrm{ex}}}{\delta_{\mathrm{W}}} = \sqrt{\frac{K_1}{\mu_0 M_{\mathrm{s}}^2}}. \tag{7}$$

For hard magnetic materials κ is on the order of unity and thus there is little difference between the

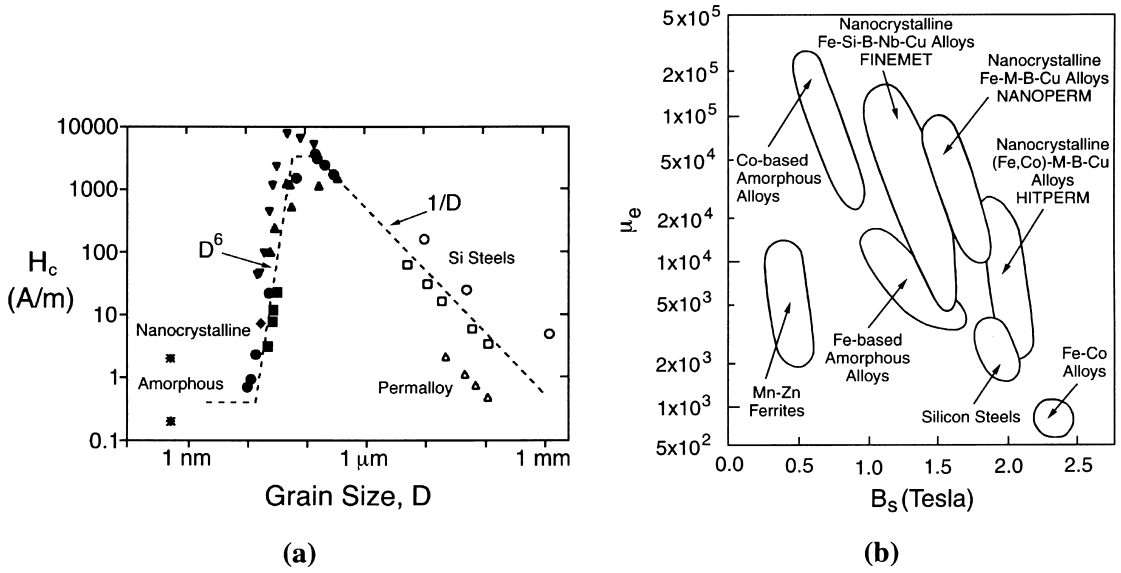

Fig. 2. (a) Herzer diagram [18] illustrating dependence of the coercivity, H_c, with grain size in magnetic alloys and (b) relationship between permeability, μ_e (at 1 kHz) and saturation polarization for soft magnetic materials [19].

ferromagnetic exchange length and the domain wall width. On the other hand, for good soft magnetic materials, where K_1 approaches zero, κ can deviate substantially from unity.

Structure sensitive magnetic properties may depend on defect concentration (point, line and planar defects), atomic order, impurities, second phases, thermal history, etc. In multi-domain materials, the *domain wall energy density*, $\gamma = 4(AK_1)^{1/2} = \gamma(x)$, is spatially varying as a result of local variations in properties due to chemical variation, defects, etc. A domain wall will prefer to locate itself in regions where the magnetic order parameter is suppressed, i.e. *pinning sites*. Since changes in induction in high-permeability materials occur by domain wall motion, it is desirable to limit variation of $\gamma(x)$ (pinning). This is one of the key design issues in developing soft magnetic materials, i.e. that of process control of the microstructure so as to optimize the soft magnetic properties. In hard materials development of two-phase microstructures with pinning phases is desirable.

For fine particle magnets the possibility of thermally activated switching and consequent reduction of the coercivity as a function of temperature must be considered as a consequence of a superparamagnetic response. This is an important limitation in magnetic recording. Superparamagnetism refers to the thermally activated switching of the magnetization over rotational energy barriers (provided by magnetic anisotropy). Thermally activated switching is described by an Arrhenius law where the activation energy barrier is $K_u\langle V\rangle$ ($\langle V\rangle$ is the switching volume). The switching frequency becomes larger for smaller particle size, smaller anisotropy energy density and at higher temperatures. Above a blocking temperature, T_B, the switching time is less than the experimental time and the magnetic hysteresis loop is observed to collapse, i.e. the coercive force becomes zero. Above T_B, the magnetization scales with field and temperature in the same manner as does a classical paramagnetic material, with the exception that the inferred dipole moment is a particle moment and not an atomic moment. Below the blocking temperature, hysteretic magnetic response is observed for which the coercivity has the temperature dependence:

$$H_c = H_{c0}\left[1 - \left(\frac{T}{T_B}\right)^{1/2}\right]. \tag{8}$$

In the theory of superparamagnetism [14, 15], the blocking temperature represents the temperature at which the metastable hysteretic response is lost for a particular experimental timeframe. In other words, below the blocking temperature hysteretic response is observed since thermal activation is not sufficient to allow the immediate alignment of particle moments with the applied field. For stability of information over ~10 years, the blocking temperature should roughly satisfy the relationship: $T_B = K_u\langle V\rangle/40k_B$. The factor of 40 [16, 17] represents $\ln(\omega_0/\omega)$, where ω is the inverse of the 10 year stability time ($\sim 10^{-4}$ Hz) and ω_0 an attempt frequency for switching (~1 GHz).

3. SOFT MAGNETIC MATERIALS

Approaches to improving intrinsic and extrinsic soft ferromagnetic properties involve (a) tailoring

Table 1. Attributes of nanocrystalline ferromagnetic materials produced by an amorphous precursor route

Alloy name	Typical composition	Nanocrystalline phase	B_s (T)	T_c (°C)
FINEMET	$Fe_{73.5}Si_{13.5}B_9Nb_3Cu_1$	α-FeSi, FeSi (DO_3)	1.0–1.2	< 770
NANOPERM	$Fe_{88}Zr_7B_4Cu$	α-Fe (b.c.c.)	1.5–1.8	770
HITPERM	$Fe_{44}Co_{44}Zr_7B_4Cu$	α-FeCo (b.c.c.), α′-FeCo (B2)	1.6–2.1	> 965

chemistry and (b) optimizing the microstructure. Significant in microstructural control has been recognition that a measure of the magnetic hardness (the coercivity, H_c) is roughly inversely proportional to the grain size (D_g) for grain sizes exceeding ~0.1–1 μm [where the D_g exceeds the domain (Bloch) wall thickness, δ_W]. Here grain boundaries act as impediments to domain wall motion, and thus fine-grained materials are usually magnetically harder than large grain materials. Significant recent development in the understanding of magnetic coercivity mechanisms has led to the realization that for very small grain sizes $D_g < \sim 100$ nm, [18], H_c decreases rapidly with decreasing grain size [Fig. 2(a)]. This can be understood by the fact that the domain wall, whose thickness, δ_W, exceeds the grain size, now samples several (or many) grains and fluctuations in magnetic anisotropy on the grain size length scale which are irrelevant to domain wall pinning. This important concept of random anisotropy suggests that nanocrystalline and amorphous alloys have significant potential as soft magnetic materials. Soft magnetic properties require that nanocrystalline grains be exchange coupled and therefore processing routes yielding free standing nanoparticles must include a compaction method in which the magnetic nanoparticles end up exchange coupled.

Random anisotropy [20, 21] has been realized in a variety of amorphous and nanocrystalline ferromagnets as illustrated in Fig. 2(b) which shows two important figures of merit for soft magnetic materials their magnetic permeability and their inductions. Combined high permeabilities and magnetic inductions are seen for amorphous Fe- and Co-based magnets with more recent improvements in the envelope occurring with the development of nanocrystalline alloys FINEMET, NANOPERM and HITPERM. The last of these combines high permeabilities, large inductions with the potential for high temperature application due to the high Curie temperature of the α′-FeCo nanocrystalline phase. Typical attributes of nanocrystalline ferromagnetic materials produced by an amorphous precursor route are summarized in Table 1 [22].

The basis for the random anisotropy model is illustrated in Fig. 3(a). The concept of a magnetic exchange length and its relationship to the domain wall width and monodomain size is important in the consideration of magnetic anisotropy in nanocrystalline soft magnetic materials. These length scales are defined by appealing to a Helmholtz free energy functional described above. These length scales again are: $\delta_W = \pi\sqrt{A/K}$ and $L_{ex} = \sqrt{A/4\pi M_s^2}$. The extension of the random anisotropy model by Herzer [18] to nanocrystalline alloys has been used as the premise for describing effective anisotropies in nanocrystalline materials. Herzer considers a characteristic volume whose linear dimension is the magnetic exchange length, $L_{ex} \sim (A/K)^{1/2}$. The unstated constant of proportionality (κ) for materials with very small K can be

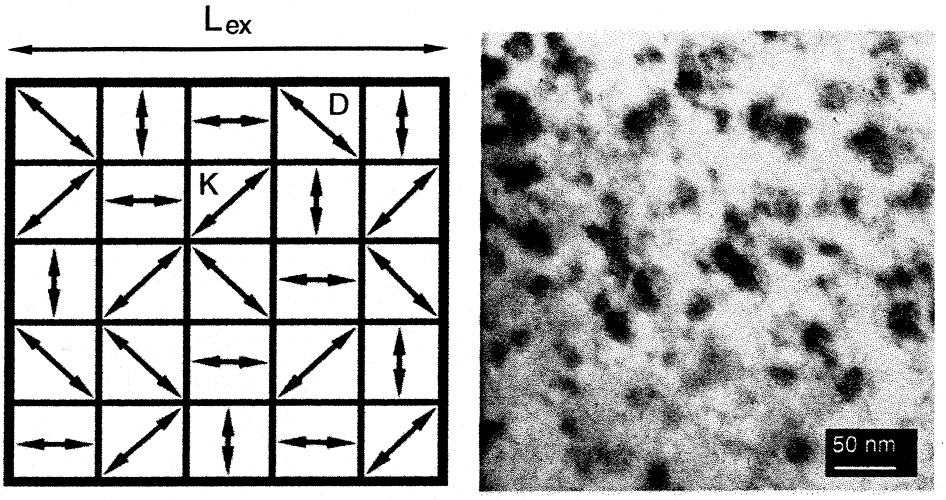

Fig. 3. (a) Cartoon illustrating N nanocrystalline grains of dimension D, in a volume L_{ex}^3. (b) TEM micrographs for an annealed $(Fe_{70}Co_{30})_{88}Hf_7B_4Cu$ HITPERM magnet ribbons [23].

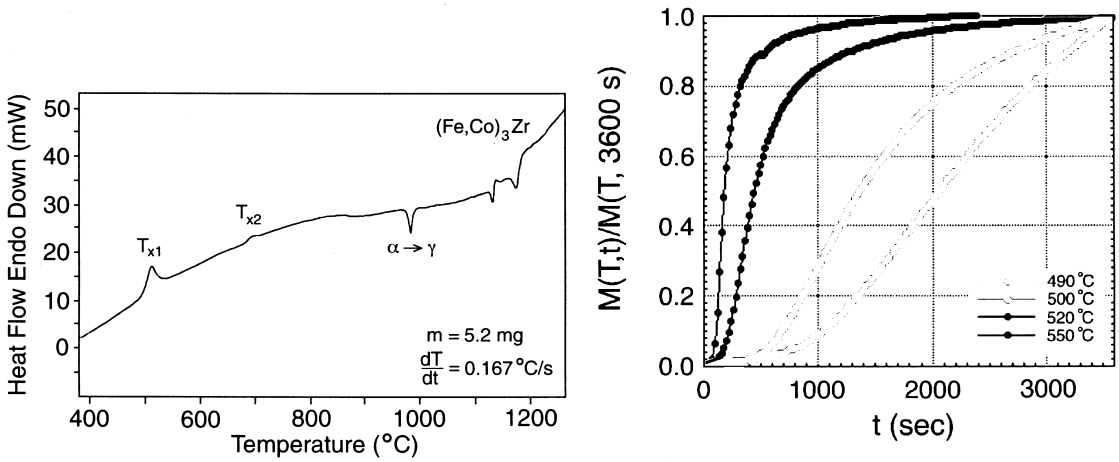

Fig. 4. (a) Differential thermal analysis (DTA) plot of heat evolved as a function of temperature for a $Fe_{44}Co_{44}Zr_7B_4Cu_1$ alloy showing two distinct crystallization events [24, 25]. (b) Isothermal magnetization as a function of time (normalized by its value after 1 h) for the NANOPERM composition $Fe_{88}Zr_7B_4Cu$ at 490, 500, 520 and 550°C, respectively [26].

quite large. The Herzer argument considers N grains, with random crystallographic easy axes, within a volume of L_{ex}^3, to be exchange coupled. For random easy axes, a random walk over all N grains yields an effective anisotropy that is reduced by a factor of $1/(N)^{1/2}$ from the value K for any one grain, thus $K_{eff} = K/(N)^{1/2}$. The number of grains in this exchange coupled volume is just $N = (L_{ex}/D)^3$, where D is the average diameter of individual grains. Treating the anisotropy self-consistently:

$$K_{eff} \sim KD^{3/2} \sim \left[\frac{K_{eff}}{A}\right]^{3/2} \sim \left[\frac{K^4 D^6}{A^3}\right]. \qquad (9)$$

Since the coercivity can be taken as proportional to the effective anisotropy, this analysis leads to yield Herzer's prediction that the effective anisotropy and therefore the coercivity should grow as the sixth power of the grain size:

$$H_c \sim H_K \sim D^6. \qquad (10)$$

Other functional dependences of the coercivity on grain size have been proposed for systems with reduced dimensionality (i.e. thin films) and supported by experimental observations. The D^6 power law is observed experimentally in a variety of alloys as illustrated in Fig. 2(a).

In FINEMET, NANOPERM and HITPERM nanocrystalline alloys, a common synthesis route has been employed resulting in a two-phase nanocrystalline microstructure. This involves rapid solidification processing of the alloy to produce an amorphous precursor. This is followed by primary (nano)crystallization of the ferromagnetic phase. For synthesis of a nanocrystalline material, the primary crystallization temperature, T_{x1}, is the useful crystallization event. In the amorphous precursor route to producing nanocrystalline materials, secondary crystallization is typically of a terminal early transition metal–late transition metal (TL–TE) and/or late transition metal–metalloid (TL–M) phase. This phase is typically deleterious in that it lowers magnetic permeability by domain wall pinning. The secondary crystallization temperature, T_{x2}, then represents the upper limit of use for nanocrystalline materials. A typical DTA study of crystallization [24, 25] is shown in Fig. 4(a).

Crystallization reactions and kinetics have been examined in some detail for certain of these alloys. For example, Hsiao *et al.* [26] has examined the crystallization kinetics of a NANOPERM alloy using magnetization as the measure of the volume fraction transformed in the primary crystallization event. Time-dependent magnetization data, at temperatures above the crystallization temperature, are illustrated in Fig. 4(b). Since the amorphous phase is paramagnetic at the crystallization temperature, the magnetization is a direct measure of the volume fraction of the α-Fe crystalline phase that has transformed. $M(t)$ then measures the crystallization kinetics. Figure 4(b) shows curves reminiscent of Johnson–Mehl–Avrami kinetics for a phase transformation. $X(t)$ has been fit to reveal activation energies of ~3.5 eV and JMA kinetic exponents of ~3/2 consistent with immediate nucleation and parabolic three-dimensional growth of nanocrystals.

Detailed studies of NANOPERM and FINEMET [27, 28] alloys have furthered the understanding of the crystallization events. Ayers *et al.* [29–31] have proposed a model based on incipient clustering of Cu in FINEMET alloys prior to nucleation of the α-FeSi ferromagnetic nanocrystalline phase. Hono *et al.*'s [32–34] atomic probe field ion microscopy (APFIM) studies of FINEMET

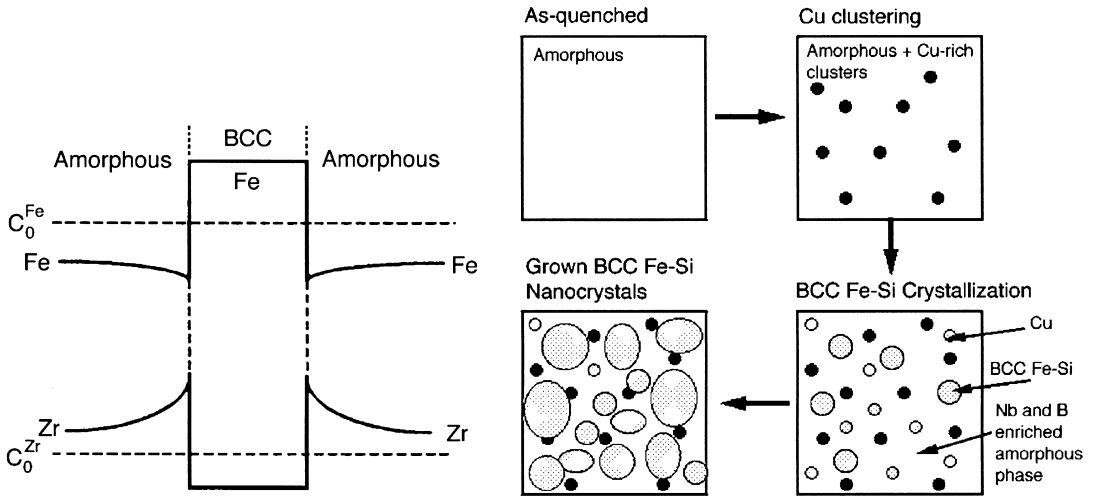

Fig. 5. (a) Schematic representation of the concentration profile of Fe and Zr near an α-Fe nanocrystal for during primary crystallization of NANOPERM type alloys [22]. (b) Proposed sequence of events in the nanocrystallization of FINEMET alloys (after Hono *et al.* [32–34]).

also supported the important role of Cu in the crystallization process, though it was thought that Fe–Si nanocrystals grew near but not necessarily on the Cu clusters [Fig. 5(b)]. Recent three-dimensional APFIM results by Hono *et al.* elegantly confirm the original Ayers mechanism. Clear inferences from magnetic measurements, EXAFS, etc. point to the role of partitioning of early transition metals and boron during primary crystallization of NANOPERM and HITPERM alloys [Fig. 5(a)].

A significant issue in the use of nanocrystalline materials in soft magnetic applications is the strength and especially the temperature dependence of the exchange coupling between the nanocrystalline grains. The intergranular amorphous phase, left after primary crystallization in FINEMET and NANOPERM, has a lower Curie temperature than the nanocrystalline ferromagnetic phase. This can give rise to exchange decoupling of the nanocrystalline grains, and resulting magnetic hardening, at relatively low temperatures. HITPERM has been developed with the aim of not only increasing the Curie temperature of the nanocrystals (in this case α′-FeCo) but also in the intragranular amorphous phase.

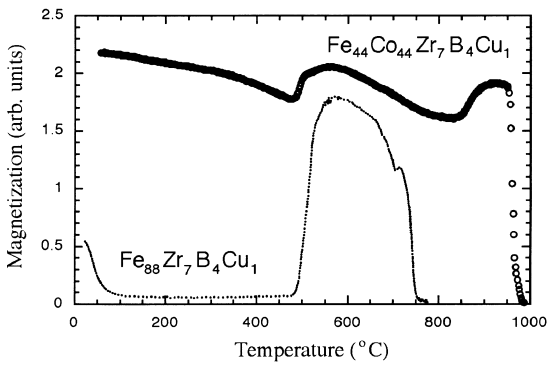

Fig. 6. (a) $M(T)$ for an alloy with a NANOPERM composition $Fe_{88}Zr_7B_4Cu$ and an alloy with a HITPERM composition, $Fe_{44}Co_{44}Zr_7B_4Cu$ [24, 25].

Figure 6(a) shows observations of magnetization as a function of temperature [22, 24, 25] for two alloys, one of a NANOPERM composition, and the other of a HITPERM composition. The amorphous precursor to NANOPERM has a T_c just above room temperature. The magnetic phase transition is followed by primary crystallization at $T_{x1} \sim 500°C$; secondary crystallization and finally T_c of the nanocrystalline α-Fe phase at ~770°C. $M(T)$ for HITPERM, shows a monotonic magnetization decrease up to T_c for the amorphous phase. Above 400–500°C structural relaxation and crystallization of the α′-FeCo phase occurs. T_{x1} is well below the Curie temperature of the amorphous phase, so that the magnetization of the amorphous phase is only partially suppressed prior to crystallization. It is this Curie temperature of the amorphous intergranular phase that is important to the exchange coupling of the nanocrystals in HITPERM.

The soft magnetic properties of nanocrystalline magnetic alloys extend to high frequencies due to the fact that the high resistivities of these alloys limit eddy current losses. Figure 7(b) illustrates the frequency dependence of the real and imaginary components of the complex permeability, μ' and μ'', for a HITPERM alloy. μ'' reflects the power loss due to eddy currents and hysteresis. The losses, $\mu''(T)$, peak at a frequency of ~20 kHz. This is reflective of the higher resistivity in the nanocrystalline materials. AC losses reflect domain wall in a viscous medium. The larger resistivity

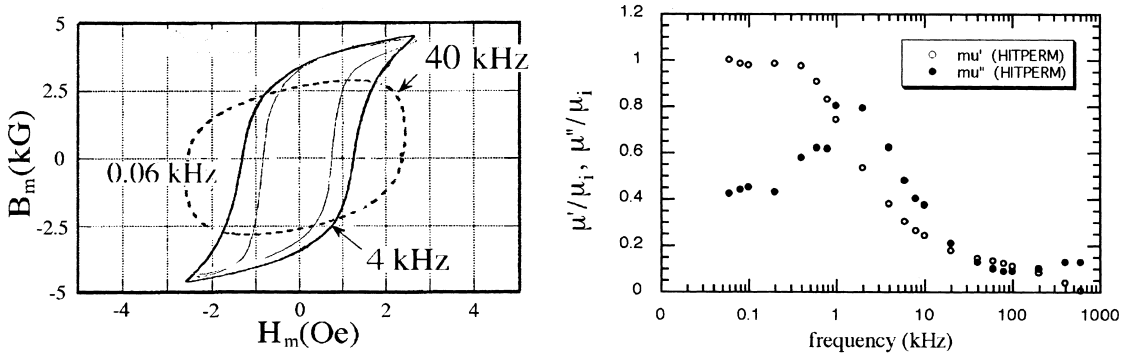

Fig. 7. AC hysteresis loops for the HITPERM alloy at 0.06, 4, 10, and 40 kHz. The sample was annealed at 650°C for 1 h and the measurements were made at room temperature with a field amplitude, $H_m = 2.5$ Oe [24, 25].

($\rho = 50\,\mu\Omega$ cm at 300 K) extends the large permeability to higher frequencies where eddy currents (classical and those due to domain wall motion) dominate the losses. The resistivity of the nanocrystalline materials is intermediate between the amorphous precursor and crystalline materials of similar composition and is a significant term in eddy current related damping of domain wall motion.

4. HARD MAGNETIC MATERIALS

Over the last few decades the most significant advancements in permanent magnet materials has come in the area of so-called rare earth permanent magnets. These have a magnetic transition metal as the majority species and a rare earth metal as the minority species. The large size difference between

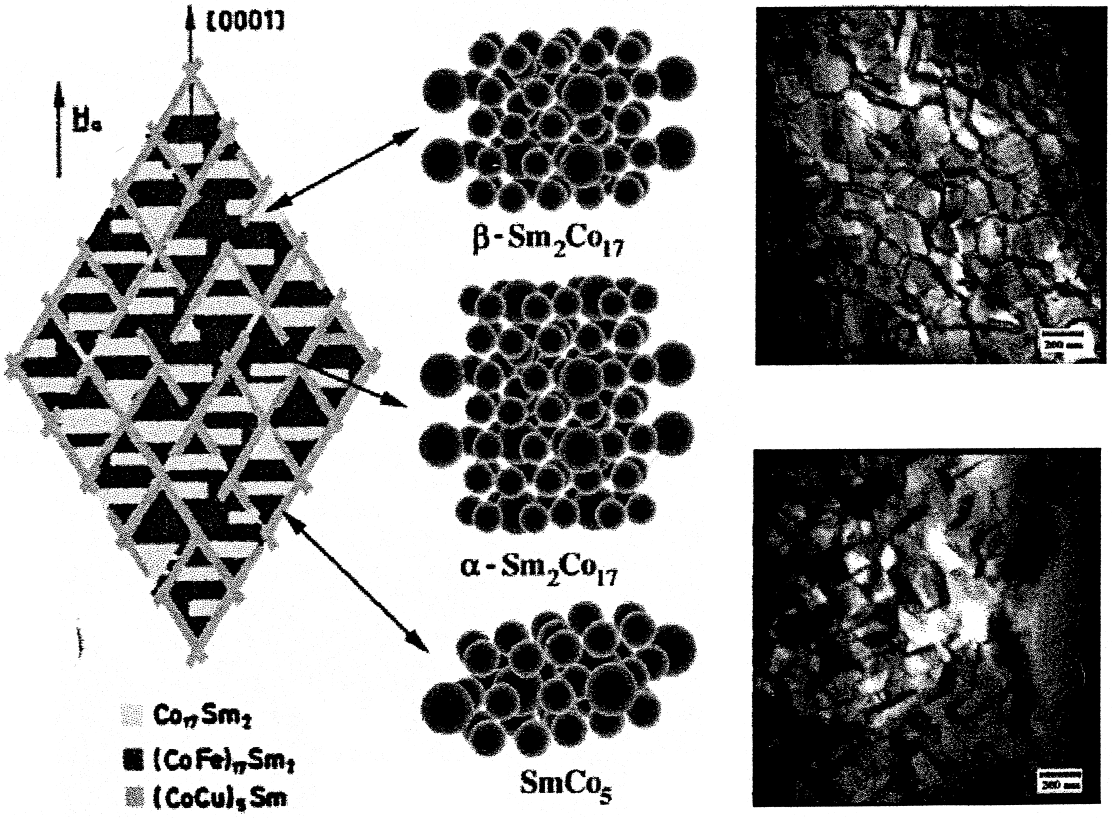

Fig. 8. (a) Cartoon showing cellular structure [48] observed in many 2:17 based magnets with cells containing the rhombohedral and hexagonal 2:17 variants and 1:5 intergranular phase; (b) crystal structures of the same and (c) TEM picture (courtesy of J. Dooley) of cellular structure observed in 2:17-based magnet.

the rare earth and transition metal species gives rise to the observation of many anisotropic crystal structures in these systems. In such systems the transition metal (TM) species is responsible for most of the magnetization and TM–TM exchange determines the Curie temperature. On the other hand the rare earth (RE) species determines the magnetocrystalline anisotropy. The anisotropic 4f-electron charge densities about the rare earth ion gives rise to large orbital moment and consequently large spin orbit interactions that are at the root of magnetocrystalline anisotropy. The development of large coercivities from materials with large (uniaxial) magnetic anisotropies involves microstructural development aimed at supplying barriers to the rotation of the magnetization and pinning of domain walls. Systems based on Sm–Co [35–38] and Fe–Nd–B [39, 40] have been of considerable recent interest.

Of the two important classes of rare earth transition metal permanent magnets, i.e. Sm–Co based and $Nd_2Fe_{14}B$ alloys [39, 40], Sm–Co alloys have much larger Curie temperatures, increasing in compounds with larger Co concentrations (e.g. the 3:29 phase). The so-called 1:5, 1:7, and 2:17 alloys and newly discovered 3:29 materials [41, 42], have received attention, where the ratios refer to the RE:TM concentrations. High Curie temperature, T_c, interstitially doped (C, N), 2:17 magnets have also been studied extensively [43–47]. The development of the Fe–Nd–B magnets has been motivated by the lower cost of Fe as compared with Co and Nd as compared with Sm. These magnets do, however, suffer from poorer high temperature magnetic properties due to their lower Curie temperatures.

The Sm_2Co_{17} phase when compared with $SmCo_5$ offers larger inductions and Curie temperatures at the expense of some magnetic anisotropy. The 2:17 materials have favorable and to date unmatched intrinsic properties: $B_r = 1.2\,T$ (25°C), intrinsic coercivity ${}_iH_c = 1.2\,T$ (25°C) and $T_c = 920°C$ (e.g. in comparison to 750°C for $SmCo_5$). The higher three-dimensional metal content (Co) leads to their high values of T_c. The 2:17 magnets currently in commercial production have a composition $Sm(CoFeCuM)_{7.5}$. Additions of Fe are made to increase the remnant induction; Cu and M (= Zr, Hf, or Ti) additions are made to influence precipitation hardening. Optimum hard magnetic properties, notably coercivities are achieved in magnets in which the primary magnetic phase has a 50–100 nm grain size (approaching the monodomain size) as described below.

Typical 2:17 Sm–Co magnets with large values of H_c are obtained through a low temperature heat treatment used to develop a cellular microstructure (see Fig. 8). Small cells of the 2:17 matrix phase are separated (and usually completely surrounded) by a thin layer of the 1:5 phase as illustrated in Fig. 8. The cell interior contains both a heavily twinned rhombohedral modification of the 2:17 phase along with coherent platelets of the so-called z-phase [48] is rich in Fe and M and has the hexagonal 2:17 structure. Typical microstructures have a 50–100 nm cellular structure, with 5–20 nm thick cell walls, and display ${}_iH_c$ of 1.0–1.5 T at room temperature. By 150°C H_c is diminished by ~50%. The loss of H_c undoubtedly continues with temperature.

In the cellular microstructure shown in Fig. 8 the magnetic anisotropy of the 1:5 cell boundary phase is important in determining the coercivity. Coercivity at room temperature in 2:17 Sm–Co magnets is largely controlled by the magnetocrystalline anisotropy of Sm^{3+} ions in $SmCo_5$ in the cell walls. In a 100 nm cellular material the room temperature coercivity is twice that of conventional 2:17 alloys. In Co-rich alloys (2:17, 3:29, etc.) development of sufficient magnetic anisotropy for hard applications is intimately related to having a preferential easy c-axis and developing a fine microstructure.

Optimization of the $Sm(CoFeCuZr)_z$ magnets discussed above have been the subject of much recent work. In particular, improvement of properties at elevated temperatures for aircraft power generators has been of particular interest [49–52]. Ma *et al.* [49] investigated the effects of intrinsic coercivity on the thermal stability of 2:17 magnets up to 450°C. Recently, Liu *et al.* [52] have investigated the role of Cu content and stoichiometry, z, on the intrinsic coercivity at 500°C in $Sm(CoFeCuZr)_z$ magnets. For magnets with $z = 8.5$, i.e. $Sm(Co_{bal}Fe_{0.1}Cu_xZr_{0.033})_{8.5}$, the optimum coercivity (4.0 T at room temperature, 1.0 T at 500°C) occurs for a Cu concentration $x = 0.088$. The role of Cu has been elucidated through microstructural studies as decreasing the cell size while concurrently increasing the density of the lamellar z-phase in these alloys.

The development of Sm–Co magnets, especially those with good high temperature magnetic properties has resulted in extensive work on a so-called 1:7 phase with a $TbCu_7$ structure [53]. $SmCo_7$ is a metastable phase at room temperature. The structures of $SmCo_7$ and Sm_2Co_{17} are both derived from the structure of $SmCo_5$. The structure of Sm_2Co_{17} can be viewed as one in which 1/3 of the Sm atoms in the $SmCo_5$ are replaced by dumbbells of Co in an ordered fashion. Kim [54, 55] have studied the intrinsic coercivity of $SmTM_7$ magnets and attributed higher coercivities at 500°C to smaller cell sizes. Recent work [54–57] on $SmCo_{7-x}Zr_x$ magnets has been extended to alloys with composition $RCo_{7-x}Zr_x$ ($x = 0$–0.8, R = Pr, Y or Er). A small amount of Zr substitution contributes to stabilization of the $TbCu_7$ structure, and improves the magneto-anisotropy field, H_A. The choice and concentration of various rare earth species influences the easy axis of magnetization.

Most recently there has been considerable interest

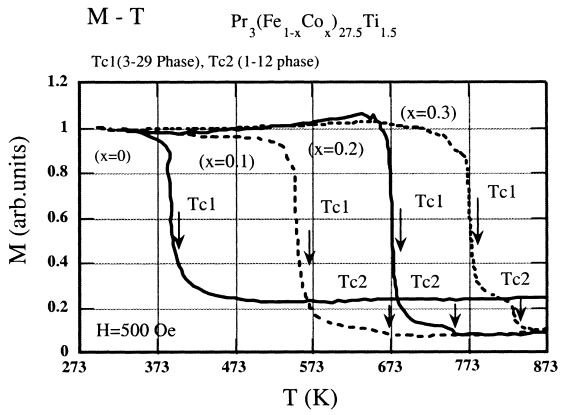

Fig. 9. $M(T)$ curves of $Pr_3(Fe_{1-x}Co_x)_{27.5}Ti_{1.5}$ as determined by thermomagnetic analysis (TMA) and showing two magnetic transitions with values of T_c denoted by T_{c1} (1:12) and T_{c2} (3:29), respectively [58, 59].

in the novel class of RE–TM intermetallics namely $RE_3(Fe, M)_{29}$ (known as 3:29 materials) and their nitrides, in potential permanent magnet applications. They are described as having a monoclinic unit cell with the A2/m space group with two formula units per unit cell. The 3:29 structure can be derived from the $REFe_5$ basis unit ($CaCu_5$-type) with replacement of RE atoms by a pair (dumbbell) of Fe atoms. The original discovery of the 3:29 phase was in a Ti-stabilized phase of composition $Pr_3Fe_{27.5}Ti_{1.5}$. With Fe as the TM species, the Curie temperatures are quite low. Promising recent developments [58, 59], however, have been reported in the $Pr_3(Fe_{1-x}Co_x)_{27.5}Ti_{1.5}$ system for x up to 0.4. Curie temperatures of up to 600°C have been reported for the $x = 0.4$ composition. See Fig. 9.

Exchange length ideas that motivate the desire for nanocrystalline microstructures can be stated for composite hard magnetic materials. These have been used to elegantly describe spring exchange magnets [60, 61]. Spring exchange magnets have particles of a hard magnetic phase in a soft magnetic matrix. See Fig. 10. The optimal size of the particles is generally in the nanometer size range, and depends on the intrinsic properties of the soft material and the anisotropy of the hard material. These magnets combine the high H_c of the hard phase and large M_s of the soft phase. In particular, exchange hardening in nanoscale composites of a soft phase and an oriented hard phase has been predicted. Magnetic hardening in $SmCo_x$–Co multilayers and nanocomposites have been observed by Liu *et al.* [62–64]. The predictions of the spring exchange model have also recently been supported in observations in FePt/Fe composite systems which are produced by solid state reaction of Fe and Pt multilayers [62–64].

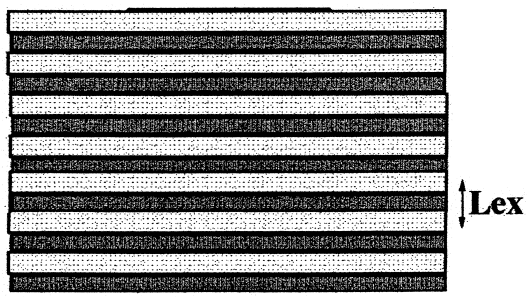

Fig. 10. (a) Multilayer structure with alternating hard and soft magnetic phases in a one-dimensional geometry of a spring exchange magnet.

5. MAGNETIC RECORDING MEDIA

Magnetic materials have a long history of use as recording media. The early tape media were composed of γ-Fe_2O_3 particles and variations of these are still used today in the tape media industry. See Ref. [65]. About two decades ago thin film media came into existence. The material used for this was Co-based alloy film. This choice is obvious in retrospect, as Co is the only one of the three common room temperature ferromagnetic elements to have uniaxial symmetry and hence be ideal for digital recording.

A typical structure of a magnetic recording medium is shown in Fig. 11. It can be seen to be composed of several layers, each of which has its own specific role to play in the production of high performance magnetic recording media. In this paper our interest lies with the magnetic layer. However, we shall see that the microstructure of the magnetic layer (and hence its properties) is controlled by that of the underlayer, so we will discuss both of these.

One other feature of thin film media must be discussed before going further, namely whether the medium has its magnetization primarily in the plane of the film or primarily out of the plane of the film. The former is called longitudinal recording and the latter perpendicular recording. Currently most, if not all, thin film media are of the longitudinal type, and it looks as if this will be the case until at least the middle of the next decade. In this section we will emphasize longitudinal media. See Fig. 11.

Over the last decade or two the main change in the requirements for longitudinal media has been the necessity to increase the storage density while maintaining and perhaps also increasing the signal to noise ratio of the media [66]. This has occurred by means of changes in the thin film media structure that were suggested by materials science input.

In order to increase the density of longitudinal recording in thin film media, it is necessary to find ways of increasing the in-plane coercivity of the media while at the same time decreasing the media grain size. The former is necessary for smaller transition lengths and hence smaller bit size and the latter is necessary for increasing the signal to noise

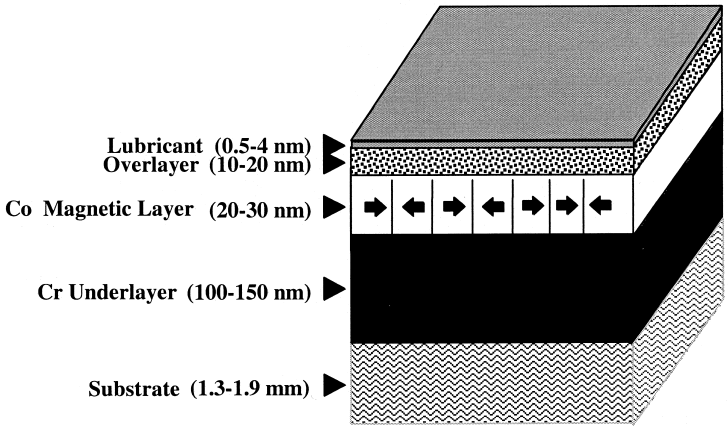

Fig. 11. Schematic of longitudinal recording media.

ratio of the thin film media. As mentioned above, the magnetic materials used as recording media are usually Co-based alloys with the h.c.p. crystal structure. Various alloy additions to the Co (Cr, Ta, Pt, etc.) change some of the intrinsic magnetic properties of the alloy. For example Pt increases the magneto-crystalline anisotropy constants of the Co-based alloy. On the other hand Cr tends to segregate to the grain boundaries of the Co alloy, thereby decreasing the exchange coupling between the grains, which in turn tends to decrease the noise of the media [67, 68]. Tantalum has been found to promote the segregation of Cr, although it does not seem to segregate itself [69]. The extrinsic properties of the alloys can be controlled by means of controlling their microstructure. As discussed above the well-known paradigm of materials science and engineering is that the extrinsic properties of materials depend on their microstructures, which in turn depends on the method by which the materials were processed. This close correlation between the properties and the processing of the thin film media gives us an important way to further develop alloys to be used in future magnetic recording devices.

In this section of the paper we will not discuss further the intrinsic properties which are affected by alloy variations of properties. Instead, we focus on the different ways of constructing thin film media that have been found to optimize their resulting magnetic properties. That is, we will be dealing with ways of changing the structure of the films that in turn will change their extrinsic magnetic properties. Features to be discussed include the grain size, crystallographic texture and elemental segregation within the magnetic media.

5.1. Grain size

The first microstructural feature we will discuss is the grain size of the magnetic film. For a given substrate temperature the grain size of a sputtered film seems to be dependent on the material constants

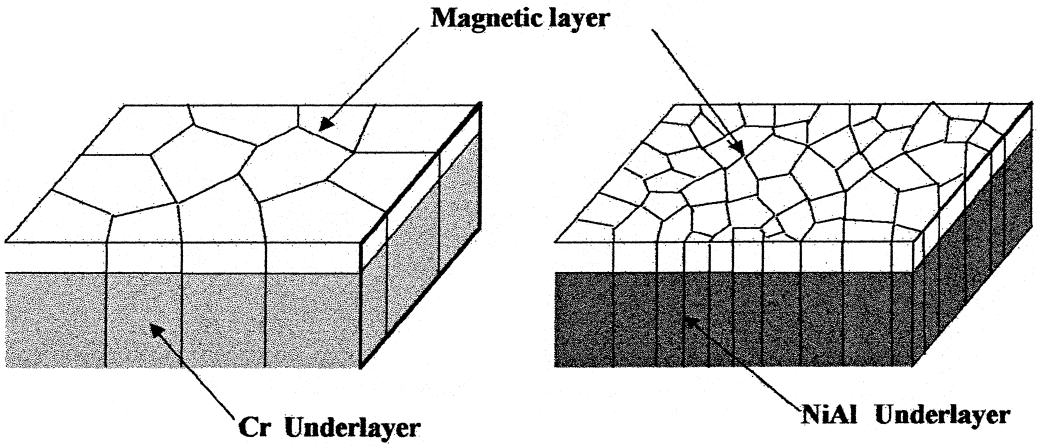

Fig. 12. Schematic showing how a smaller grain size underlayer gives rise to a smaller grain size magnetic layer.

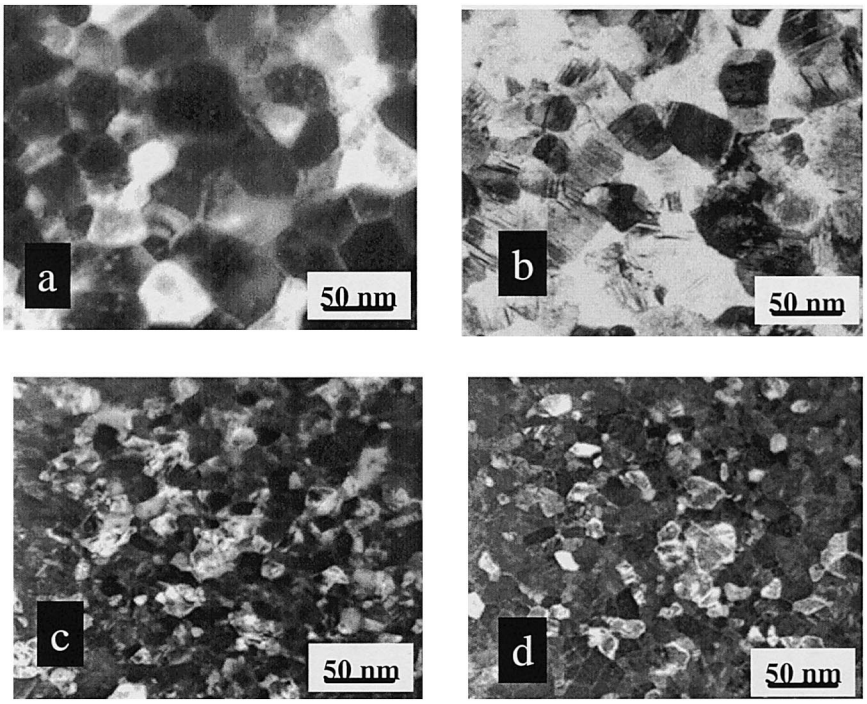

Fig. 13. Comparison of the grain size of the underlayers and magnetic layer. (a) Cr layer and (b) corresponding Co alloy thin film. (c) NiAl underlayer and corresponding Co alloy thin film. Note that the smaller grain size of the NiAl (c) gives rise to a smaller grain size of the Co alloy. Cf. (d) and (b).

such as thermal diffusivity, atomic mobility, etc. However when a material is sputtered onto a crystalline film the new film tends to replicate the grain size of the existing film. See Fig. 12. Most longitudinal media are sputtered onto crystalline underlayers, which until recently have been mainly Cr or Cr-based b.c.c. alloys. Thus, for the case of the magnetic film it tends to take on the grain size of the underlayer. The invention of Lee *et al.* of NiAl underlayers [70] was successful in part because of the intrinsically smaller grain size of the NiAl underlayer thin films. See Fig. 13. This is due to the strong bonding in the intermetallic phase inhibiting grain growth.

Grain size is important because written bites of information should contain at least about 50 magnetic grains so as to obtain a reasonable signal to noise ratio. As the grain size decreases, the same number of grains can be in smaller written bites, which means for a given amount of media noise more information can be written on the magnetic thin film. There is a limit however as to how small the grain size can be. As grains get smaller and smaller thermal fluctuations become important. The way to overcome this is to move to higher magnetocrystalline anisotropy materials such as CoSm or CoPt alloys. See below.

Another important microstructural feature is the grain size distribution. The sharper the distribution the better is the resulting media. This is because grains of the same size will switch at the same time, giving rise to a very square hysteresis loop. One of the reasons for the success of NiAl underlayers is that they form with more uniform grain size than Cr thin films. This can be seen from Fig. 13.

5.2. *Crystallographic texture*

Another important structural feature is the crystallographic texture of the magnetic material. For longitudinal media it is desirable to have as many of the grains as possible with their *c*-axes in the plane of the film. However, when h.c.p. Co or one of its alloys is sputter deposited on an amorphous substrate such as NiP or glass, the newly developed Co alloy film usually takes on a crystallographic texture such that its *c*-axis is perpendicular to the plane of the film. This is believed to be due to the fact that the growing film seeks to minimize its total surface free energy and the close packed planes (which have the lowest specific surface energy) of the h.c.p. structure are the (0001) basal planes. Because the *c*-axis is the magnetic easy axis for h.c.p. Co, this is ideal for perpendicular recording in which the magnetization should be perpendicular to the film. The texture of such films has been optimized by the use of underlayers, or as they are sometimes called for perpendicular media, seedlayers.

Since most recording media today are longitudinal in nature (that is the magnetization vectors lie in the plane of the film) it is necessary to find a way

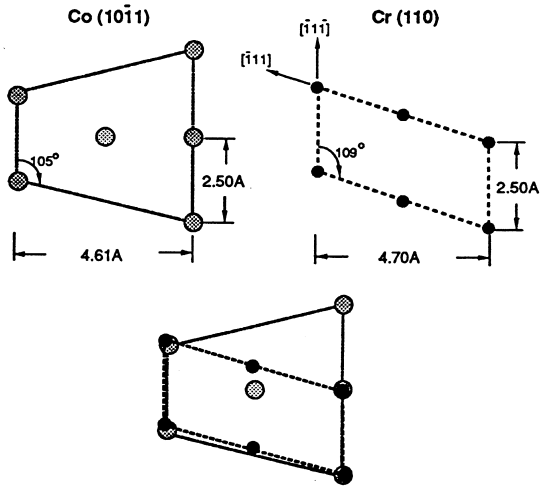

Fig. 14. Schematic showing the epitaxial relationship of $(10\bar{1}1)_{Co}//(110)_{Cr}$. For this orientation relationship the c-axis is out of the plane.

to insure that most of the magnetic thin films grains are in that orientation. In order to obtain films with their c-axes in the plane of the film different schemes have been devised to optimize the crystallographic texture, including the use of underlayers. The earliest methods used were to sputter deposit Cr as an underlayer to the Co-based alloy films. When Cr is deposited on an amorphous substrate (such as NiP) at ambient temperature, it grows with a {110} crystallographic texture. This crystallographic texture develops because the {110} surfaces of the grains are closest packed, and hence should have the lowest surface energy. This makes them favorable over the other low index planes. When Co alloys are deposited on Cr underlayers with the crystallographic texture {110} the epitaxial relationship:

$$(10\bar{1}1)_{Co}//(110)_{Cr}$$

develops, see Fig. 14. This has been discussed in detail [71, 72].

The crystallographic c-axis is out of the plane of the film (the angle between the $(10\bar{1}1)$ and the [0001] is 28°). This is not ideal for in-plane magnetization. The next advance in the construction of magnetic thin films was to sputter deposit the Cr underlayers at elevated temperatures, that is by depositing the films on a heated substrate. This results in Cr underlayers with (002) crystallographic textures. By means of epitaxy it is possible to get the $(11\bar{2}0)$ Co plane to lie in the plane of the film, causing the closest packed plane of Co [the (0001) plane] to lie parallel to the closest packed plane of Cr (the {110} planes). This forces the c-axes of these planes to lie in the plane of the film. Thus, by suitable manipulation of the processing conditions (in this case the preheating temperature of the substrate) it is possible to obtain Co-based thin films with most grains having their c-axes in the film plane.

In the mid-1990s Lee *et al.* [70, 73, 74] developed a new class of underlayers, namely those with the B2 structure. This structure is a crystallographic derivative of the b.c.c. (A2) structure and has the space group $Pm\bar{3}m$; prototype CsCl. Since its lattice parameter is nearly the same as that of b.c.c. Cr, epitaxial relations that occur between Co-based alloys and Cr should also occur between Co-based alloys and NiAl. Sputter deposited NiAl on glass substrates have produced films with grain sizes that are nearly half the diameter of comparable Cr underlayers.

Although the B2 structure is similar to the A2 structure, a different crystallographic texture is obtained, namely the {211} texture. This texture

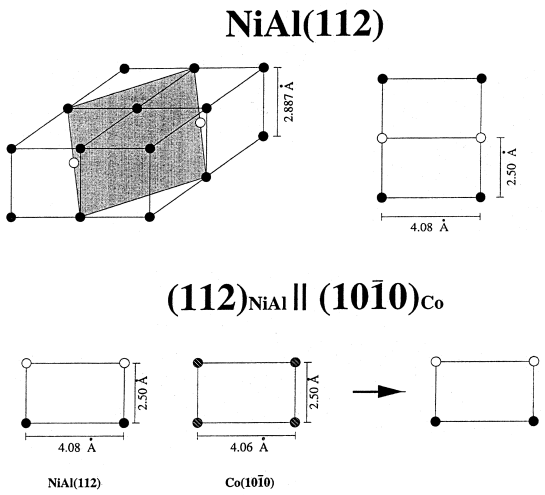

Fig. 15. Schematic showing the $(112)_{NiAl}$ planes and their epitaxial relationship with the $(10\bar{1}0)_{Co}$.

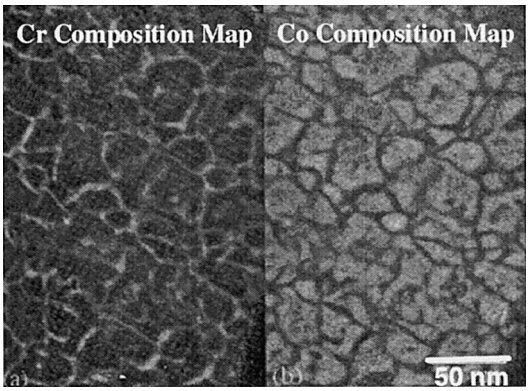

Fig. 16. Cr and Co distribution maps from a Co-based alloy thin film. Notice the enhancement of Cr to the grain boundaries. After Wittig *et al.* [82].

allows for the orientation relationship:

$$(10\bar{1}0)_{Co}//(112)_{B2}.$$

See Fig. 15 for a schematic of this orientation relationship. Since in this case only one orientation variant per underlayer grain is obtained, this crystallographic texture is more favored than the $(11\bar{2}0)_{Co}//(002)_{Cr}$ one.

Thus, the control of the crystallographic orientation of the magnetic layer is obtained by controlling the crystallographic orientation of the underlayer, which in turn can be optimized by its deposition conditions [75]. The polycrystalline magnetic layer is often grown epitaxially grain to grain on the underlayer. The mechanism of producing the orientation of choice for the magnetic layer is "epitaxial" nucleation on the underlayer. This epitaxial relationship also gives rise to the size of the grains of the magnetic layer.

5.3. Chemical segregation

A final feature of the films will be discussed, namely elemental segregation. Such segregation is thought to be a major contributor to the decrease in exchange coupling among the Co alloy grains. Exchange coupling among the Co grains plays a significant role in determining the magnetic and recording properties of Co-alloy thin films. A Co-alloy magnetic thin film with smaller exchange coupling usually has larger H_c, lower squareness and smaller media noise. Non-magnetic alloying elements, such as Cr, Mn, W and B, have been found to effectively reduce the exchange coupling in Co-based alloys as determined by δM and media noise measurements. On the other hand, while Pt significantly increases the magneto-crystalline anisotropy, it also appears to promote a more exchange coupled medium.

The observation of compositional inhomogeneity was first observed by Maedia *et al.* in 1985. They observed that Cr segregation in CoCr thin films using TEM with selected-chemical-etching sample preparation [67]. Later, other techniques were utilized to analyze compositional inhomogeneity in the Co-based alloys such as CoCrPt and CoCrTa. These techniques include nano probe X-ray energy dispersive spectroscopy (EDS) [68], nuclear magnetic resonance (NMR) [76], thermal magnetic analysis [77], ferromagnetic resonance (FMR) [78], atom probe field ion microscopy (APFIM) [79] and XAFS [69, 80]. Each of these techniques has confirmed the existence of enriched Cr regions in the thin film which contribute to their magnetic properties. More recently Yahisa *et al.* [81] and Wittig *et al.* [82] have presented Co and Cr composition maps using energy-filtered TEM imaging. See Fig. 16. The segregation of the Cr atoms to the Co alloy grain boundaries is evident. The Cr diffuses from the interiors of the grains to the grain boundaries and also may diffuse up the grain boundaries from the Cr-based underlayer. Besides Cr, elements such as Ta, Nb, B and Mn (from the CrMn underlayers, proposed by Lee *et al.*) are believed to reduce the exchange coupling. It is not clear whether these or other elements actually segregate to the Co alloy grain boundaries or if they drive other alloying elements (such as Cr) to do so, which in turn provides for the isolation of the grains [83, 84]. Also, it is not obvious which elements are effective in reducing exchange coupling. Studies such as the above mentioned demonstrate that the distribution of chemical species in a film is an important feature that can be used to manipulate the properties of the thin films. Thus, the distribution of the elements in a thin film should be included in the features that we normally term "microstructural", which control the extrinsic properties of materials.

5.4. Future media

Although h.c.p. Co-based alloys have been in use for over two decades, it seems clear that they will need to be replaced in the future by media that has higher magnetocrystalline anisotropy. This is because that in order to allow for greater recording densities, the grain sizes of the media have been decreasing. If the grains are isolated from one another the possibility exists that they will reach the size at which they become superparamagnetic. This loss of thermal stability can be overcome by increasing the magnetocrystalline anisotropy of the media. High anisotropy media like CoSm, CoPt and FePt with anisotropy constants an order of magnitude larger than Co alloy films are candidates for such extremely high density recording media. However, many problems must be overcome with these alloys before they take their place as media.

Another possible future media is the so-called "patterned media" in which a periodic array of magnetic particles on a flat surface is utilized to

store information. Much research is underway to develop methods for such nano-engineering. See a recent review by Chou [85].

6. SUMMARY

We have given a brief survey of the way that the structure of magnetic materials has evolved over the last decade. As with most advances in materials science, progress has been made after a thorough understanding of the important microstructural features of a material which affect their properties have determined followed by changing the way that material is produced.

Acknowledgements—We wish to thank the Air Force Office of Scientific Research, Air Force Material Command, USAF, who sponsored much of our recent work on nanocrystalline materials, under grant number F49620-96-1-0454. D.E.L. thanks the CMU Data Storage Systems Center for long-term support through the National Science Foundation under Grant No. ECD-8907068 and also support from a NEDO grant. M.E.M. thanks the National Science Foundation for support through NYI award DMR-9258450, grant award DMR-95000313 and grant award DMR-9803700. We also thank our many students and postdoctoral associates for their work.

REFERENCES

1. Gleiter, H., *Prog. Mater. Sci.*, 1989, **33**, 223.
2. McHenry, M. E., Majetich, S. A., De Graef, M., Artman, J. O. and Staley, S. W., *Phys. Rev. B*, 1994, **49**, 11358.
3. McHenry, M. E., Gallagher, K., Johnson, F., Scott, J. H. and Majetich, S. A., in *Recent Advances in the Chemistry and Physics of Fullerenes and Related Materials*, *ECS Symposium Proceedings*, Pennington, NJ, PV 96-10, ed. K. M. Kadish and R. S. Ruoff, 1996, p. 703.
4. McHenry, M. E. and Subramoney, S., *Fullerenes: Chemistry, Physics and Technology*, ed. K. M. Kadish and R. S. Ruoff. John Wiley, in press.
5. McHenry, M. E., Willard, M. A., Iwanabe, H., Sutton, R. A., Turgut, Z., Hsiao, A. and Laughlin, D. E., *Bull. Mater. Sci.*, 1999, **22**, 495.
6. Turgut, Z., Huang, M.-Q., Gallagher, K., Majetich, S. A. and McHenry, M. E., *J. appl. Phys.*, 1997, **81**, 4039.
7. Turgut, Z., Scott, J. H., Majetich, S. A. and McHenry, M. E., *I.E.E.E. Trans. Magn.*, 1998, **83**, 6468.
8. Turgut, Z., Nuhfer, N. T., Piehler, H. R. and McHenry, M. E., *J. appl. Phys.*, 1999, **85**, 4406.
9. Coey, J. M. D., *Rare-Earth Iron Permanent Magnets*. Clarendon Press, Oxford, 1996.
10. Skomski, R. and Coey, J. M. D., *Phys. Rev. B*, 1993, **48**, 15812.
11. Chikazumi, S., *Physics of Magnetism*. Kreiger, Malabar, FL, 1978.
12. Cullity, B. D., *Introduction to Magnetic Materials*. Addison-Wesley, Reading, MA, 1972.
13. Coey, J. M. D., *Rare-Earth Iron Permanent Magnets*. Clarendon Press, Oxford, 1996.
14. Bean, C. P. and Livingston, J. D., *J. appl. Phys.*, 1959, **30**, 120S.
15. Jacobs, I. S. and Bean, C. P., in *Magnetism*, Vol. 3, ed. G. T. Rado and H. Suhl. Academic Press, New York, 1963.
16. Lu, P.-L. and Charap, S. H., *I.E.E.E. Trans. Magn.*, 1994, **30**, 4230.
17. Charap, S. H., Lu, P.-L. and He, Y., *I.E.E.E. Trans. Magn.*, 1997, **33**, 978.
18. Herzer, G., in *Handbook of Magnetic Materials*, ed. Buschow, K.H.J., Vol. 10, Chap. 3, 1997, p. 415. Elsevier Science, Amsterdam.
19. Makino, A., Suzuki, K., Inoue, A. and Masumoto, T., *Mater. Trans. JIM*, 1991, **32**, 551.
20. Alben, R., Budnick, J. and Cargill III, G. S., in *Metallic Glasses*. ASM, Metals Park, OH, 1978, p. 304.
21. Alben, R., Becker, J. J. and Chi, M., *J. appl. Phys.*, 1978, **49**, 1653.
22. McHenry, M. E., Willard, M. A. and Laughlin, D. E., *Prog. Mater. Sci.*, 1999, **44**, 291.
23. Iwanabe, H., Lu, B., McHenry, M. E. and Laughlin, D. E., *J. appl. Phys.*, 1999, **85**, 4424.
24. Willard, M. A., Laughlin, D. E., McHenry, M. E., Thoma, D., Sickafus, K., Cross, J. O. and Harris, V. G., *J. appl. Phys.*, 1998, **84**, 6773.
25. Willard, M. A., Huang, M.-Q., Laughlin, D. E., McHenry, M. E., Cros, J. O., Harris, V. G. and Franchetti, C., *J. appl. Phys.*, 1999, **85**, 4421.
26. Hsiao, A., Turgut, Z., Willard, M. A., Selinger, E., Lee, M., Laughlin, D. E., McHenry, M. E. and Hasegawa, R., *MRS Res. Symp. Proc.*, 1999, **577**, 551.
27. Yoshizawa, S. Y., Oguma, S. and Yamauchi, K., *J. appl. Phys.*, 1988, **64**, 6044.
28. Yoshizawa, Y., Yamauchi, K., Yamane, T. and Sugihara, H., *J. appl. Phys.*, 1988, **64**, 6047.
29. Ayers, J. D., Harris, V. G., Sprague, J. C. and Elam, W. T., *Appl. Phys. Lett.*, 1994, **64**, 974.
30. Ayers, J. D., Konnert, J. H., Dantonio, P., Pattnaik, A., Vold, C. L. and Jones, H. N., *J. Mater. Sci.*, 1995, **30**, 4492.
31. Ayers, J. D., Harris, V. G., Sprague, J. C., Elam, W. T. and Jones, H. N., *Acta mater.*, 1998, **46**, 1861.
32. Hono, K., Inoue, A. and Sakurai, T., *Appl. Phys. Lett.*, 1991, **58**(19), 2180.
33. Hono, K., Hiraga, K., Wang, Q., Inoue, A. and Sakurai, T., *Acta metall. mater.*, 1992, **40**, 2137.
34. Hono, K., Zhang, Y., Tsai, A. P., Inoue, A. and Sakurai, T., *Scripta metall. mater.*, 1995, **32**, 131.
35. Wallace, W. E., Strnat, K. J., Hoffer, G., Olson, J. C., Ostertag, W. and Becker, J. J., *J. appl. Phys.*, 1967, **38**, 1001.
36. Wallace, W. E., in *Rare Earth Intermetallics*. Academic Press, New York, 1973, p. 171.
37. Wallace, W. E. and Nasasimhan, K. S. V. L., in *The Science and Technology of Rare Earth Materials*. Academic Press, New York, 1980, p. 393.
38. Strnat, K., in *Ferromagnetic Materials*, Vol. 4, ed. E. P. Wohlfarth and K. H. J. Buschow. Amsterdam Publishers, Amsterdam, 1988, p. 131.
39. Croat, J. J., Herbst, J. F., Lee, R. W. and Pinkerton, F. E., *J. appl. Phys.*, 1984, **55**, 2078.
40. Sagawa, M., Tenaud, P., Vial, F. and Hiraga, K., *I.E.E.E. Trans. Magn.*, 1984, **MAG-26**, 1957.
41. Cadogan, J. M., Li, H. S., Margarian, A., Dunlop, J. B., Ryan, D. H., Collocot, S. J. and Davis, R. L., *J. appl. Phys.*, 1994, **76**, 6138.
42. Kalogirou, O., Psycharis, V., Gjoka, M. and Niarchos, D., *J. Magn. Magn. Mater.*, 1995, **147**, L7.
43. Otani, Y., Hurley, D. F. P., Sun, H. and Coey, J. M. D., *J. appl. Phys.*, 1991, **69**, 5584.
44. Kou, X. C., Grossinger, R., Katter, M., Wecker, J., Schultz, L., Jacobs, T. H. and Buschow, K. H. J., *J. appl. Phys.*, 1991, **70**, 2274.
45. Li, H. S. and Coey, J. D. M., in *Magnetic Materials*

6, ed. K. H. J. Buschow. Elsevier Science, Amsterdam, 1991.
46. Hadjipanayis, G. C., Zheng, Y. H., Murthy, A. S., Gong, W. and Yang, F. M., *J. Alloys Comp*., 1995, **222**, 49.
47. Grossinger, R., Kou, X. C., Jacobs, T. H. and Buschow, K. H. J., *J. appl. Phys*., 1991, **69**, 5596.
48. Fidler, J. and Skalicky, P., *J. Magn. Magn. Mater*., 1982, **27**, 127.
49. Ma, B. M., Liang, Y. L. and Bounds, C., *J. appl. Phys*., 1997, **81**, 5612.
50. Wong, B. Y., Willard, M. and Laughlin, D. E., *J. Magn. Magn. Mater*., 1997, **169**, 178.
51. Chen, J. X., Liu, J. F., Ni, C. and Hadjipanayis, G. C., *J. appl. Phys*., 1998, **83**, 7139.
52. Liu, J. F., Ding, Y., Zhang, Y., Dimitar, D., Zhang, F. and Hadjipanayis, G. C., *J. appl. Phys*., 1999, **85**, 5660.
53. Buschow, K. H. and den Broeder, F. J. A., *J. less-common Metals*, 1973, **3**, 191.
54. Kim, A. S., *J. appl. Phys*., 1997, **81**, 5609.
55. Kim, A. S., *J. appl. Phys*., 1997, **83**, 6715.
56. Huang, M. Q., Wallace, W. E., McHenry, M. E., Chen, Q. and Ma, B. M., *J. appl. Phys*., 1998, **83**, 6718.
57. Huang, M. Q., Drennan, M., Wallace, W. E., Chen, Q., Ma, B. M. and McHenry, M. E., *J. appl. Phys*., 1999, **85**, 5663.
58. Shah, V. R., Markandeyulu, G., Rama Rao, K. V. S., Huang, M. Q., Sirisha, K. and McHenry, M. E., *J. Magn. Magn. Mater*., 1998, **190**, 233.
59. Shah, V. R., Markandeyulu, G., Rama Rao, K. V. S., Huang, M. Q., Sirisha, K. and McHenry, M. E., *J. appl. Phys*., 1999, **85**, 4678.
60. Kneller, E. F. and Hawig, R., *I.E.E.E. Trans. Magn*., 1991, **27**, 3588.
61. Skomski, R. and Coey, J. M. D., *Phys. Rev. B*, 1993, **48**, 15812.
62. Liu, J. P., Liu, Y., Skomski, R. and Sellmyer, D. J., *J. appl. Phys*., 1999, **85**, 4812.
63. Sellmyer, D. J., Yu, M. and Kirby, R. D., *Nano-98*, 1998.
64. Sellmyer, D. J., Yu, M., Thomas, R. A., Liu, Y. and Kirby, R. D., *Phys. Low-Dim. Struct*., 1998, **1/2**, 155.
65. Bate, G., in *Ferromagnetic Materials*, Vol. 2, ed. E. P. Wohlfarth. North-Holland, Amsterdam, 1980, pp. 381–507.
66. Lambeth, D. N., Yang, W., Gong, H., Laughlin, D. E., Lu, B., Lee, L.-L., Zou, J. and Harllee, P. S., *Proc. MRS*, 1998, **517**, 181.
67. Maeda, Y., Hirono, S. and Asahi, M., *Japan. J. appl. Phys*., 1985, **24**(12), L951.
68. Chapman, J. N., McFadyen, I. R. and Bernades, J. P. C., *J. Magn. Magn. Mater*., 1986, **62**, 359.
69. Kemner, K. M., Harris, V. G., Chakarian, V., Idzerda, Y. U., Elam, W. T., Kao, C.-C., Feng, Y. C., Laughlin, D. E. and Woicik, J. C., *J. appl. Phys*., 1996, **79**, 5345.
70. Lee, L.-L., Laughlin, D. E. and Lambeth, D. N., *I.E.E.E. Trans. Magn*., 1994, **MAG-30**(5), 3951.
71. Hono, H., Wong, B. and Laughlin, D. E., *J. appl. Phys*., 1990, **68**(4), 734.
72. Wong, B. Y. and Laughlin, D. E., *Appl. Phys. Lett*., 1992, **61**, 2533.
73. Lee, L.-L., Laughlin, D. E. and Lambeth, D. N., *J. appl. Phys*., 1997, **81**(8), 4366.
74. Lee, L.-L., Cheong, B. K., Laughlin, D. E. and Lambeth, D. N., *Appl. Phys. Lett*., 1995, **67**(24), 3638.
75. Hsu, Y.-N., Laughlin, D. E. and Lambeth, D. N., *Proc. MRS*, 1998, **517**, 199.
76. Yoshida, K., Kakibayashi, H. and Yasuoka, H., *J. appl. Phys*., 1990, **68**, 705.
77. Maeda, Y. and Takahashi, M., *J. appl. Phys*., 1990, **68**, 4751.
78. Bernades, J. B. C., Schrauwen, C. P. G. and Van Kesteren, H. W., *I.E.E.E. Trans. Magn*., 1990, **26**, 33.
79. Hono, K., Maeda, Y., Li, J.-L. and Sakurai, T., *I.E.E.E. Trans. Magn*., 1993, **29**, 3745.
80. Kemner, K. M., Harris, V. G., Elam, W. T. and Lodder, C. J., *I.E.E.E. Trans. Magn*., 1994, **30**, 4017.
81. Yahisa, Y., Kimoto, K., Usami, K., Matsuda, Y., Inagak, J., Furusawa, K. and Narishige, S., *I.E.E.E. Trans. Magn*., 1995, **31**, 2836.
82. Wittig, J. E., Nolan, T. P., Ross, C. A., Schabes, M. E., Tang, K., Sinclair, R. and Bentley, J., *I.E.E.E. Trans. Magn*., 1998, **34**, 1564.
83. Deng, Y., Lambeth, D. N. and Laughlin, D. E., *I.E.E.E. Trans. Magn*., 1993, **29**(5), 3676.
84. Feng, Y. C., Laughlin, D. E. and Lambeth, D. N., *I.E.E.E. Trans. Magn*., 1994, **30**(6), 3948.
85. Chou, S. Y., *Proc. I.E.E.E*., 1997, **85**(4), 652.